Philosophical Magazine Letters
Vol. 90, No. 5, May 2010, 337–347

Taylor & Francis
Taylor & Francis Group

Effects of annealing temperature on structural, optical, and electrical properties of antimony-doped tin oxide thin films

V. Senthilkumar[a], P. Vickraman[a]*, J. Joseph Prince[b], M. Jayachandran[c] and C. Sanjeeviraja[d]

[a]*Department of Physics, Gandhigram Rural University, Gandhigram 624302, Tamil Nadu, India;* [b]*Department of Physics, Anna University, Tiruchirappalli 620024, Tamil Nadu, India;* [c]*Electrochemical Material Science Division, Central Electrochemical Research Institute, Karaikudi 630006, Tamil Nadu, India;* [d]*Department of Physics, Alagappa University, Karaikudi 630003, Tamil Nadu, India*

(*Received 29 May 2009; final version received 26 January 2010*)

Antimony-doped tin oxide (ATO) films, approximately 320 nm in thickness, have been prepared by electron beam evaporation onto glass substrates. The films were annealed at temperatures between 400°C and 550°C in air and their structure and surface morphologies were observed by X-ray diffraction (XRD) and atomic force microscopy (AFM) after the different annealing treatments. XRD patterns of the ATO thin films as-deposited and annealed at 400°C showed that they were amorphous, but annealing beyond 400°C caused the films to become polycrystalline with tetragonal structure and orientated in the (1 1 0) direction. The grain size in the annealed films, obtained from the XRD analysis, was in the range 146–256 Å and this increased with the annealing temperature. The dislocation density, cell volume and strain were found to decrease gradually with increasing annealing temperature. Photoluminescence spectra revealed an intensive blue/violet peak at 420 nm, which increased gradually in height with annealing. It is suggested that an increase in the population of Sb^{+5} ions might be the reason for the enhancement of the blue/violet emission. The optical properties of the films were also investigated in the UV-visible-NIR region (300–1000 nm). The optical constants, namely the refractive index n and the extinction coefficient k in the visible region were calculated. The optical energy band gap, as determined by the dependence of the absorption coefficient on the photon energy at short wavelengths, was found to increase from 3.59 to 3.76 eV with annealing temperature.

Keywords: annealing process; X-ray diffraction; photoluminescence; atomic force microscopy; optical properties

1. Introduction

The search for new innovative materials for applications has created a platform for electrically conducting highly transparent thin films that have great promise for use

*Corresponding author. Email: vrsvickraman@yahoo.com

ISSN 0950–0839 print/ISSN 1362–3036 online

DOI: 10.1080/09500831003662529
http://www.informaworld.com

in optoelectronic devices. Tin oxide (SnO_2) is an interesting semiconductor having a wide band gap (3.6 eV) and the highest carrier mobility among the oxide materials [1]. Owing to the inherent wide band gap, the material has its absorption edge beyond the Visible spectral region [2]. SnO_2 is stable within a broad spectrum of high temperatures and shows excellent resistance to strong acids and bases. Its mechanical integrity is exemplified by good adhesion to many types of substrates [3]. The desirable properties of SnO_2 have led many researchers to study pure and doped films and to evaluate their use as electrodes in thin-film photovoltaic solar cells [4]. The synthesis of antimony-doped tin oxide (ATO) has been achieved by employing several techniques, i.e., sputtering [5], spray pyrolysis [6], sol–gel [7], dip coating from chemical solutions [8], and electron-beam evaporation [9]. In this article, we report an investigation of the effect of annealing on the structural, optical, and electrical properties of ATO prepared by electron beam evaporation.

2. Experimental details

ATO (1 at.%) thin films were prepared by electron beam evaporation. A co-precipitated powder was calcinated at 500°C for 5 h, and then palletized and used as source material for evaporation. The vacuum chamber was evacuated to a base pressure of 5×10^{-5} mbar. Glass slides were used as substrates. The substrates were cleaned using a liquid detergent, and then agitated ultrasonically in acetone before rinsing with distilled water. The temperature of the heated substrates was measured using a thermocouple in contact with the substrate holder. The substrate temperature was kept at 250°C during the film deposition process. The film thickness was measured using a stylus profilometer.

The structural properties of the as-deposited films were studied by an X-ray diffractometer (PANalytical-X'pert pro, with Cu-Kα radiation at $\lambda = 0.15418$ nm) in the 2θ range 10–80°. Morphological features were studied with a PicoSPM Picoscan 2100 atomic force microscope (AFM). The chemical state of the elements in the ATO films were analyzed from XPS spectra using a Multilab 2000 X-ray photoelectron spectroscope. The photoluminescence (PL) was recorded using a Carry Eclipse fluorescence spectrometer (VARIAN) employing a PbS-photodetector and a 150 W Xe arc discharge lamp as the excitation light source. Optical transmission of the films in the wavelength range of 300–1000 nm relative to air was determined using a UV-Vis-NIR double-beam spectrophotometer (Carry 500 – VARIAN).

3. Results and discussion

The X-ray diffraction (XRD) patterns of the ATO thin films, as-deposited and annealed at temperatures of 400°C, 450°C, 500°C, and 550°C for 90 min, recorded in air, are shown in Figure 1a. The XRD pattern associated with the film annealed at 400°C shows a predominantly amorphous structure, while that associated with the film annealed at 450°C displays reflections related to a crystallographic phase. These reflections become progressively more intense and sharper in the films annealed at higher temperatures. All the peaks' positions agree well with the standard ATO tetragonal structure (JCPDS card no. 88-2348). No phase that could

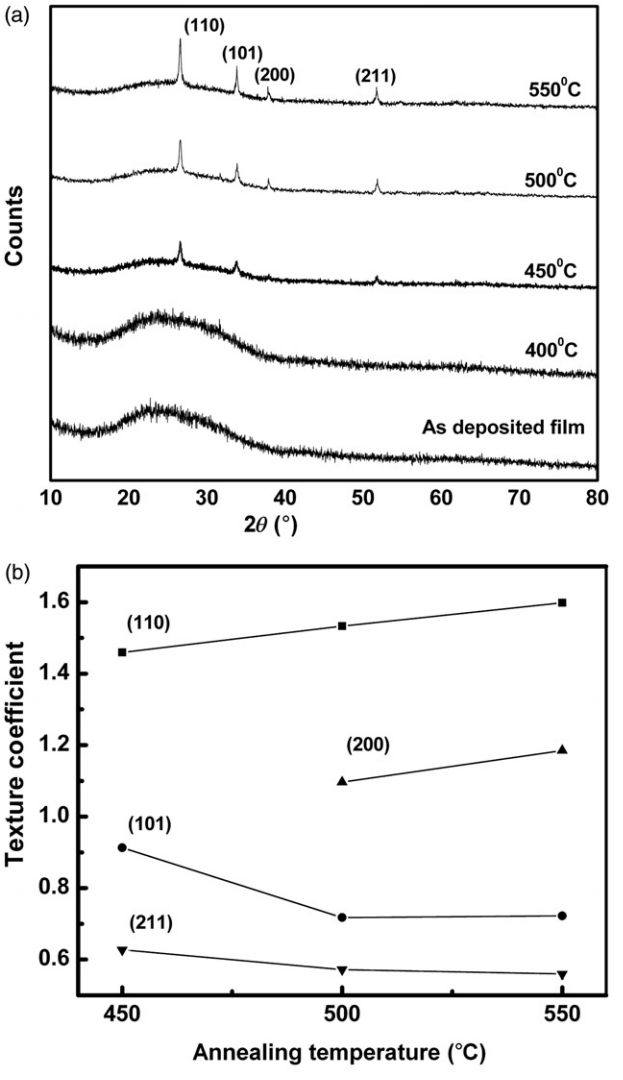

Figure 1. (a) XRD pattern and (b) variation of texture coefficient with annealing temperature for ATO films deposited by electron beam evaporation.

be ascribed to the compounds of antimony is detected in the XRD spectra, suggesting that all the antimony ions might have been accommodated into the lattice of the SnO_2 as a substitute for tin ions [10]. The intensity distributions of these reflections reveal that the films have a preferred crystallographic orientation along the (1 1 0) diffraction plane. This preferred orientation was also found for ATO films prepared by RF sputtering [11] and plasma-enhanced chemical vapor deposition [3]. The lattice parameters (a and c), grain size D, dislocation density δ, cell volume v, and strain ε [12] have been calculated for the (1 1 0) prominent reflection plane and are presented in Table 1. The lattice constants are found to agree well with the bulk

Table 1. Structural parameters of ATO thin films annealed at different temperatures (T_A).

				Lattice parameters (Å)					
T_A (°C)	2θ	d (Å)	$[hkl]$	a	c	D (Å)	Cell volume V (cm^3)	$\delta \times 10^{15}$ (lines cm^{-2})	$\varepsilon \times 10^{-3}$
400	–	–	–	–	–	–	–	–	–
450	26.56	3.3533	110	4.74	3.19	146	71.88	4.65	4.79
500	26.57	3.3510	110	4.74	3.19	208	71.83	2.30	3.29
550	26.56	3.3530	110	4.73	3.18	256	71.63	1.51	2.67

values ($a = 4.73$ Å and $c = 3.18$ Å). The sizes of grains in the films increase with an increase in the annealing temperature. This is mainly due to an increase in the thermal energy for crystallization, recrystallization, and growth of grains in the films. Structural parameters, such as dislocation density δ and micro-strain ε are found to show a decreasing trend with increase in the annealing temperature, which might result from a reduction in the concentration of lattice imperfections.

The preferential orientation of the films is studied by calculating the texture coefficient TC(hkl) for all the planes using the equation [13]:

$$\mathrm{TC}(hkl) = \frac{I(hkl)/I_0(hkl)}{(1/N)\sum(I(hkl)/I_0(hkl)}, \tag{1}$$

where TC(hkl) is the texture coefficient of the (hkl) plane, I is the measured intensity, I_0 is the JCPDS standard intensity for the corresponding powder, and N is the number of reflections observed in the XRD pattern. The variations in texture coefficient have been calculated for all the diffraction peaks, i.e., the (1 1 0), (1 0 0), (2 0 0), and (2 1 1) planes (Figure 1b). It is observed that the (1 1 0) plane has a high texture coefficient of 1.59 for a film annealed to 550°C whereas it is low and tends to decrease linearly for the (2 1 1) plane, which suggests that the maximum preferred orientation of the films along the (1 1 0) diffraction plane is associated with the increased number of grains within that plane.

Figures 2a and b represents AFM images of ATO films doped with 1 at.wt% of antimony as-deposited and annealed at 550°C for 90 min. It is found that as-deposited films show smooth surfaces whereas the annealed film has rougher surfaces with larger grains. This reveals that an increase in annealing temperature improves the crystallinity of films. The average roughness of the films is found to be 14.7 and 17.2 nm, respectively, for images a and b. The observed grain sizes are observed to be much higher than those measured by XRD. Since XRD provides a measure of the grain size normal to the films while AFM gives a surface profile of the film, it might be reasonably concluded that the grains are either not spherical, or are spherical but larger at the surface of the film.

Figure 3a shows the XPS survey scan spectrum of an ATO film annealed at 550°C. The measured binding energies of $Sn3d_{5/2}$, $Sn3d_{3/2}$, and O 1s at 486.15, 494.6, and 530 eV, respectively, are consistent with results reported elsewhere [14].

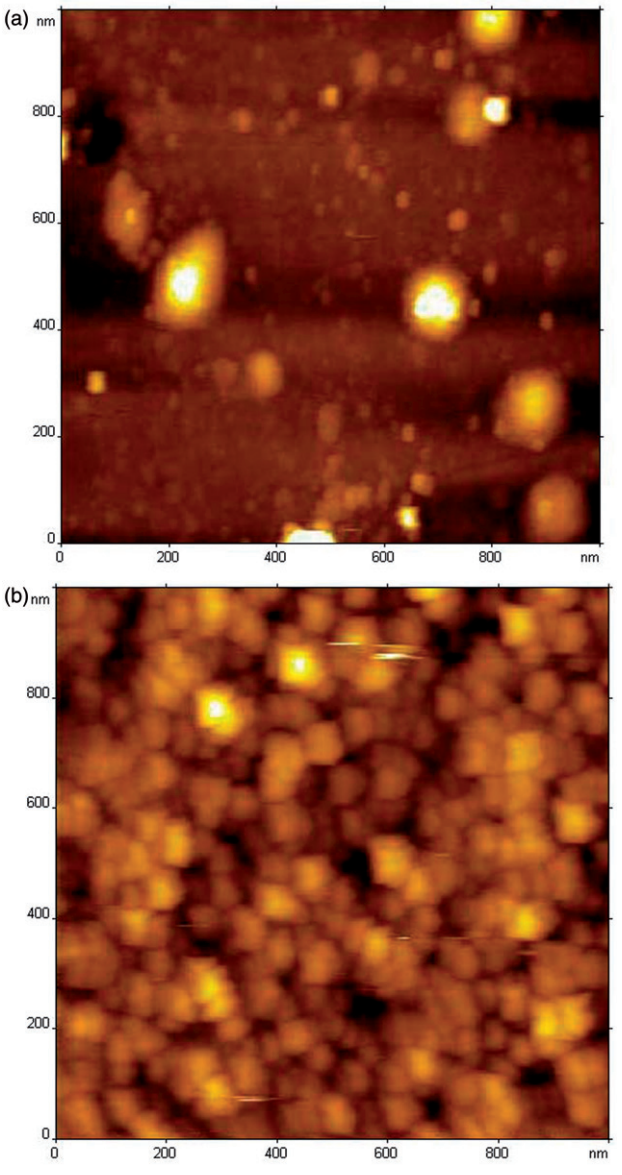

Figure 2. (Color online). AFM image of ATO thin films: (a) as-deposited and (b) annealed at 550°C.

The binding energy difference of 8.4 eV between the $Sn3d_{5/2}$ and $Sn3d_{3/2}$ doublet levels is assigned to Sn in SnO_2, SnO (or) Sn. Owing to the low-doping concentration of Sb, no trace of a peak is observed for $Sb3d_{3/2}$ in the survey spectra. The $Sb3d_{5/2}$ peak is found in the region of the O 1s peak because its binding energy (530.3 eV) lies close to the binding energy of O 1s which is deduced from a Gaussian fit. Image (b)

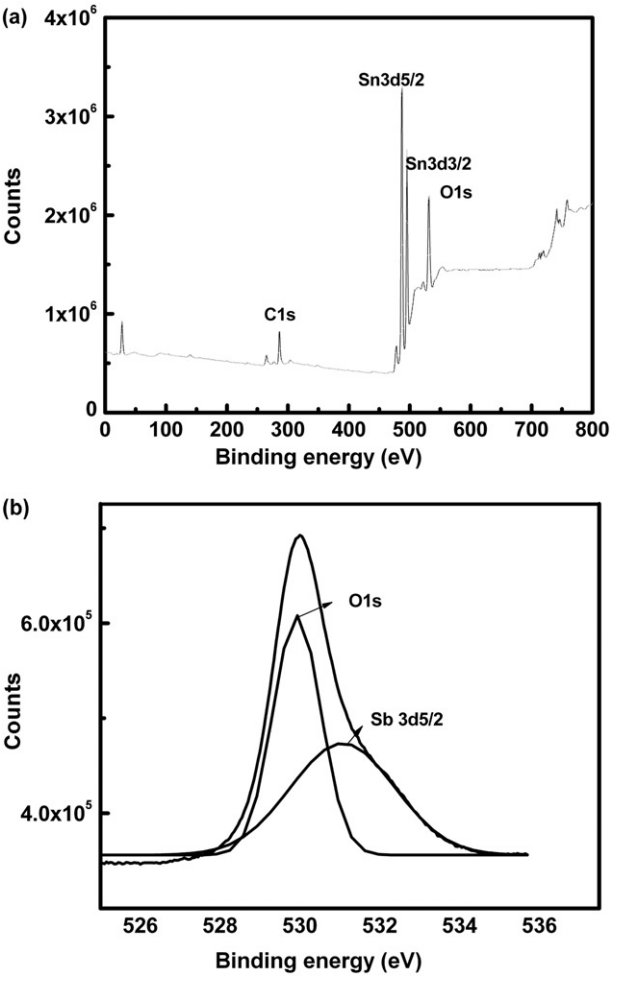

Figure 3. XPS survey scan spectra of ATO films annealed at 550°C (a) for the whole spectra and (b) for O 1s + Sb3d5/2 XPS.

illustrates the binding energy of $Sb3d_{5/2}$ which appears at 531.07 eV, indicating the presence of Sb^{+5} state in Sb_2O_5.

Figure 4 shows the PL spectra of the ATO thin films. It is observed that a blue/violet peak at 420 nm is present for the as-grown and all the annealed samples. The intensity of this peak increases gradually on increasing the annealing temperature. Blue/violet peaks at 400 and 430 nm for undoped SnO_2 have been reported by several researchers [15,16]. Chang et al. [17] observed a luminescence peak at 2.95 eV from undoped SnO_2 powder and suggested that the origin of blue/violet luminescence peak of undoped SnO_2 arises from oxygen vacancies, tin interstitials or dangling bonds, and other structural defects. In general, in polycrystalline oxide thin films/powders, oxygen vacancies are known to be the

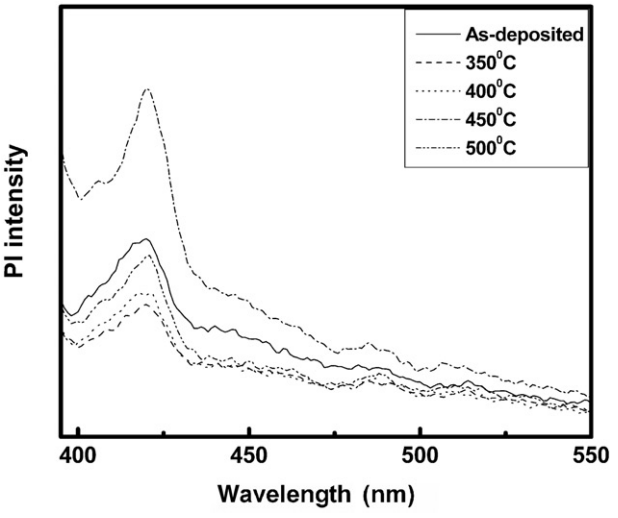

Figure 4. Room temperature photoluminescence spectrum of ATO thin films annealed at different temperatures.

most common defect and form a donor level [18]. In this study, Sb ion doping is shown to alter the characteristic property of the host atoms by creating acceptor and donor Sb^{+3} and Sb^{+5} ions, which lead to electron transitions that is suggested to be the reason for the appearance of the blue/violet peak. The increase in the peak intensity with annealing is shown in Figure 5. Annealing may be expected to decrease the density of defects and improve the crystal orientation, thereby reducing the non-radiative recombination and leading to an increase in the intensity of the blue/violet peak. Also, as a consequence of an increase in oxidation processes, the Sb^{+5} ion population is enhanced, which again leads to an increase in the blue/violet emission as shown in Figure 4.

The transmittance spectra of ATO films as-deposited and annealed at the temperatures of 400°C, 450°C, 500°C, and 550°C in the air under atmospheric conditions are shown in Figure 5a. The films are highly transparent over the visible and near-infrared regions, but the optical transmission falls very sharply near the UV region owing to the onset of fundamental absorption. The spectra show a high transmission for films annealed at 550°C, an effect that is attributed to less scattering, structural homogeneity, and better crystallinity [19]. The spectral shift towards the UV region may be attributed to the improved crystallinity and a higher concentration of carriers [20]. Furthermore, the fundamental absorption edge is shifted toward the shorter wavelength side with the increase of annealing temperature suggesting that the widening of the energy gap in the films may arise from a Moss–Burstein shift [21].

Figures 5b and c shows the plots of refractive index and extinction coefficient as a function of wavelength λ for the 1 at.wt % ATO film. The transmission performance is related to the refractive index and the extinction coefficient.

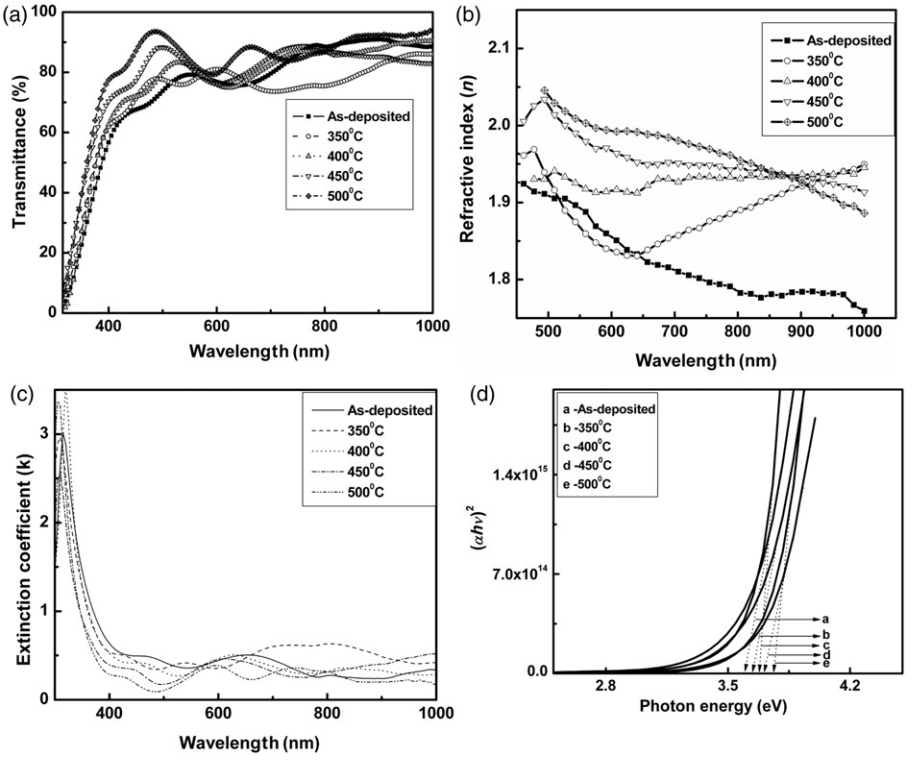

Figure 5. Optical properties of ATO films with different annealing temperatures: (a) transmission spectra, (b) refractive index n, (c) extinction coefficient k, and (d) variation of $(\alpha h\upsilon)^2$ with photon energy.

The refractive index n is evaluated from the measured transmittance versus wavelength [22]:

$$n^2(\lambda) = H + \sqrt{H^2 - n_0^2(\lambda) n_s^2(\lambda)}$$
$$H = \frac{1}{2}\left(n_0^2(\lambda) + n_s^2(\lambda)\right) + 2n_0 n_s \left[\frac{T_{\max} - T_{\min}}{T_{\max} T_{\min}}\right]. \tag{2}$$

Here, n_s (=1.5) is the refractive index of the glass substrate.

The values of the extinction coefficient k are calculated using the equation:

$$k = \frac{\alpha\lambda}{4\pi}. \tag{3}$$

The effects of annealing on the refractive index and the extinction coefficient of the ATO films are shown in Figures 5a and b. The refractive index increases from 1.87 to 2.0 on raising the annealing temperature from 400°C to 550°C, which may be attributed to an increase in the packing density and the crystallinity of the film.

Table 2. Optical constants, n and k, at 550 nm, and the optical band gap E_g for as-deposited and annealed ATO thin films.

Annealing temperature (°C)	Optical band gap E_g (eV)	Refractive index n	Extinction coefficient k
As-deposited film	3.59	1.89	0.362
400	3.64	1.87	0.413
450	3.67	1.92	0.300
500	3.71	1.98	0.311
550	3.76	2.00	0.268

The variation of absorption co-efficient with photon energy for direct band-to-band transitions is given by the relation $\alpha h\upsilon = A(h\upsilon - E_g)^n$ where $h\upsilon$ is the photon energy, E_g is the energy difference between conduction and valence bands, n is 1/2 for allowed transitions, and 3/2 for forbidden transitions. Figure 5d shows a plot of $(\alpha h\upsilon)^2$ versus photon energy values for the ATO films. Values of E_g are determined by extrapolating the linear portion of these curves to zero absorption and are presented in Table 2. An increase in the band gap from 3.59 to 3.76 eV with increase of annealing temperature is observed. The values of E_g found are close to reported values of 3.1–4.1 eV [7,23,24]. Huang et al. [20] reported a similar type of variation of optical band gap with annealing temperature in RF sputtered ATO thin films. The variation of optical band gap is attributed to the improved crystallinity and higher concentrations of carriers which leads to a rise of Fermi level within the conduction band producing electrically degenerate semiconductors [19,20].

The electrical resistivity of ATO films as a function of annealing temperature is shown in Figure 6a. It is observed that the electrical resistivity decreases with the increase in annealing temperature. This might be partly due to the increase in carrier concentration. At lower annealing temperature, fine grains are formed because of a relatively low thermal energy. However, at higher annealing temperature, the surface mobility of constituent elements increases and grain growth is favored. An increase in carrier mobility may arise from an increase in the crystallinity of the films on annealing. Schottky barriers cause the grain boundary to have a lower conductivity than that inside the grain. As the annealing temperature increases, it is proposed that a higher concentration of carriers as well as a higher mobility both contribute to the decrease in the electrical resistivity.

Devices using transparent conductors require high electrical conductivity and optical transmission. Scropp et al. [25] suggested a figure of merit F for conductivity and optical transmission which are inversely proportional to each other. It is reported that the performance of such device is solely dependent upon higher values of F, which is defined as

$$F = -\frac{1}{(\rho \ln T)}, \tag{4}$$

where T is the transmittance and ρ is the electrical resistance. The figure of merit (Figure 6b) of the ATO films is found to increase from $3.3 \times 10^2\,\Omega^{-1}\,\mathrm{cm}^{-1}$ to

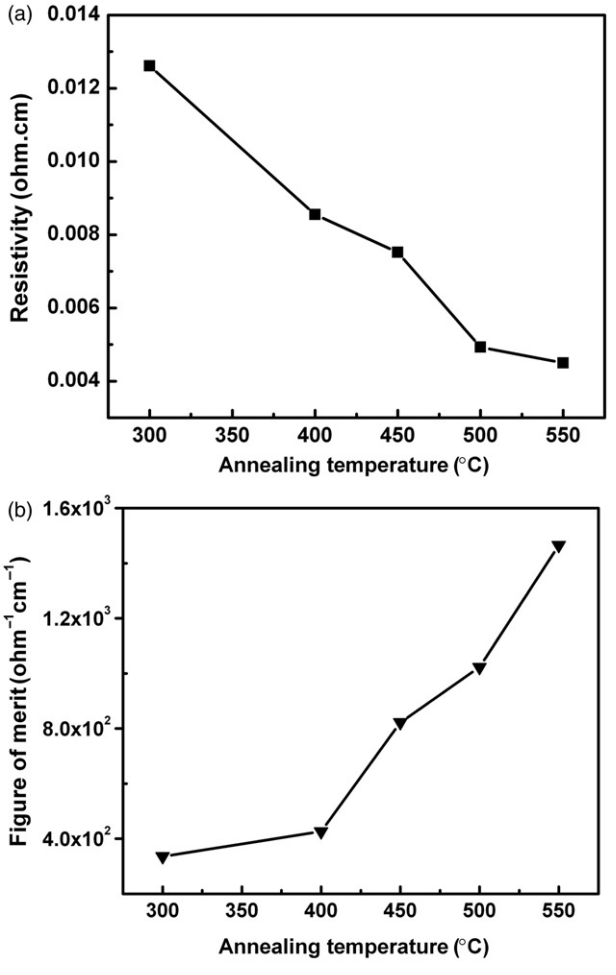

Figure 6. Variation with different annealing temperatures of (a) electrical resistivity, and (b) figure of merit of ATO thin films.

$1.46 \times 10^3\,\Omega^{-1}\,\mathrm{cm}^{-1}$ on increasing the annealing temperature. This arises from the decrease in the electrical resistivity. The highest value of the figure of merit $1.465 \times 10^3\,\Omega^{-1}\,\mathrm{cm}^{-1}$ occurs for the film annealed at 550°C in air.

4. Conclusions

Highly transparent and nanostructured ATO thin films were prepared by electron beam evaporation technique. The structural and optical properties of these films were studied as a function of annealing temperature. The grain size increased with

the annealing temperature while the cell volume, dislocation density, and strain decreased. The optical band gap energy of evaporated and annealed films lies in the range 3.59–3.76 eV. A widening of the band gap in the films on annealing is ascribed to a Moss–Burstein shift. The refractive index and extinction coefficient at 550 nm decreased with the annealing temperature from 2.0 to 1.89 and from 0.362 to 0.268, respectively. Also, on annealing, the electrical resistivity of the films decreased, which is interpreted in terms of an increase in the mobility and the carrier density. The highest value of the figure of merit $1.46 \times 10^3\,\Omega^{-1}\,\mathrm{cm}^{-1}$ was obtained for the film annealed at 550°C. It is concluded that the effect of annealing temperature can play a pivotal role in controlling the structural, electrical, and optical properties of ATO thin films.

References

[1] D. Szczuko, J. Werner and S. Oswald, Appl. Surf. Sci. 179 (2001) p.301.
[2] E. Shanti, V. Dutta, A. Banerjee and K.L. Chopra, J. Appl. Phys. 51 (1980) p.6243.
[3] K.S. Kim, S.Y. Yoon, W.J. Lee and K.H. Kim, Surf. Coat. Tech. 138 (2001) p.229.
[4] E. Elangovan and K. Ramamurthi, Cryst. Res. Tech. 38 (2003) p.779.
[5] S. Jäger, B. Szyszka, J. Szyczyrbowski and G. Bräuer, Surf. Coat. Tech. 98 (1998) p.1304.
[6] S. Shanthi, C. Subramanian and P. Ramasamy, J. Cryst. Growth 197 (1999) p.858.
[7] C. Terrier, J.P. Chatelon and J.A. Roger, Thin Solid Films 295 (1997) p.95.
[8] M.I.B. Bernardi, L.E. Soledade, I.A. Santos, E.R. Leite, E. Longo and J.A. Varela, Thin Solid Films 405 (2002) p.228.
[9] E.K.H. Shokr, Semicond. Sci. Tech. 15 (2000) p.247.
[10] J. Rockenberger, U. Fedle, M. Tisher, L. Troger, M. Haase and H. Weller, J. Chem. Phys. 112 (2000) p.4296.
[11] J. Ma, Y. Wang, F. Ji, X. Yu and H. Ma, Mater. Lett. 59 (2005) p.2142.
[12] N.S. Ramgir, Y.K. Hwang, I.S. Mulla and J.S. Chang, Solid State Sci. 8 (2006) p.359.
[13] C. Barrett and T.B. Massalski, *Structure of Metals*, Pergamon Press, Oxford, 1980, p.1923.
[14] J.Y.W. Seto, J. Appl. Phys. 46 (1975) p.5247.
[15] F. Gu, S. Wang, M.K. Lu, X.F. Cheng, S.W. Liu, G.J. Zhou, D. Xu and D.R. Yuan, J. Cryst. Growth 262 (2004) p.182.
[16] S.S. Chang and D.K. Park, Mater. Sci. Eng., B 95 (2002) p.55.
[17] S.S. Chang, S.O. Yoon and H.J. Park, Cer. Int. 31 (2005) p.405.
[18] J. Jin, C.S. Pyung, C.C. Ik, S.D. Chan, P.J. Sung, B.T. Lee and P. Yeong-jun, Solid State Commun. 127 (2003) p.595.
[19] J.J. Prince, S. Ramamurthy, B. Subramanian, C. Sanjeeviraja and M. Jayachandran, J. Cryst. Growth 240 (2002) p.142.
[20] J.-L. Huang, Y. Pan, J.Y. Chang and B.S. Yau, Surf. Coat. Tech. 184 (2004) p.188.
[21] E. Burstein, Phys. Rev. 93 (1952) p.632.
[22] R. Swanepoel, J. Phys. E Sci. Instrum. 16 (1983) p.1214.
[23] T.D. Senguttuvan and L.K. Malhotra, Thin Solid Films 289 (1996) p.22.
[24] E.K. Shokr, Semicond. Sci. Tech. 15 (2000) p.247.
[25] R.E.I. Scropp, C.E. Matovich, P.K. Bhatt and A.K. Madan, in *20th IEEE Photovoltaic Specialists Conference*, Las Vegas, USA, 1988.